Monthly Notices of the ROYAL ASTRONOMICAL SOCIETY

MNRAS **527,** 2065–2070 (2024) https://doi.org/10.1093/mnras/stad3267
Advance Access publication 2023 October 25

The updated BaSTI stellar evolution models and isochrones – IV. α-Depleted calculations

Adriano Pietrinferni,[1★] Maurizio Salaris,[1,2] Santi Cassisi,[1,3] Alessandro Savino,[4] Alessio Mucciarelli,[5,6] David Hyder[2] and Sebastian Hidalgo[7,8]

[1]*INAF – Osservatorio Astronomico di Abruzzo, Via M. Maggini s/n, I-64100 Teramo, Italy*
[2]*Astrophysics Research Institute, Liverpool John Moores University, 146 Brownlow Hill, Liverpool L3 5RF, UK*
[3]*INFN – Sezione di Pisa, Largo Pontecorvo 3, I-56127 Pisa, Italy*
[4]*Department of Astronomy, University of California, Berkeley, Berkeley, CA 94720, USA*
[5]*Dipartimento di Fisica e Astronomia 'Augusto Righi', Alma Mater Studiorum, Universitá di Bologna, Via Gobetti 93/2, I-40129 Bologna, Italy*
[6]*INAF – Osservatorio di Astrofisica e Scienza dello Spazio di Bologna, Via Gobetti 93/3, I-40129 Bologna, Italy*
[7]*Instituto de Astrofisica de Canarias, Via Lactea s/n, La Laguna, Tenerife, 38205, Spain*
[8]*Department of Astrophysics, University of La Laguna, Via Lactea s/n, La Laguna, Tenerife, 38205, Spain*

Accepted 2023 October 19. Received 2023 October 19; in original form 2023 September 13

ABSTRACT

This is the fourth paper of our new release of the BaSTI (a Bag of Stellar Tracks and Isochrones) stellar model and isochrone library. Following the updated solar-scaled, α-enhanced, and white dwarf model libraries, we present here α-depleted ([α/Fe] $= -0.2$) evolutionary tracks and isochrones, suitable to study the α-depleted stars discovered in Local Group dwarf galaxies and in the Milky Way. These calculations include all improvements and updates of the solar-scaled and α-enhanced models, and span a mass range between 0.1 and 15 $M_{\odot}$, and 21 metallicities between [Fe/H] $= -3.20$ and $+0.45$ with a helium-to-metal enrichment ratio $\Delta Y/\Delta Z = 1.31$, homogeneous with the solar-scaled and α-enhanced models. The isochrones – available in several photometric filters – cover an age range between $\sim$20 Myr and 14.5 Gyr, including the pre-main-sequence phase. We have compared our isochrones with independent calculations of α-depleted stellar models, available for the same α-element depletion adopted in the present investigation. We have also discussed the effect of an α-depleted heavy element distribution on the bolometric corrections in different wavelength regimes. Our α-depleted evolutionary tracks and isochrones are publicly available at our BaSTI website.

Key words: stars: evolution – stars: horizontal branch – Hertzsprung–Russell and colour–magnitude diagrams – stars: interiors.

1 INTRODUCTION

Extended (in terms of mass and chemical composition ranges) and accurate sets of stellar model calculations are fundamental inputs to a wide variety of numerical tools employed to interpret spectroscopic and photometric observations of individual stars, star clusters, and galaxies, both resolved and unresolved.

In the last few years, we have undertaken a massive update – in terms of physics inputs and parameter space coverage – of our BaSTI (a Bag of Stellar Tracks and Isochrones) stellar models and isochrone library, and published in Paper I (Hidalgo et al. 2018) a new grid of solar-scaled models and isochrones, in Paper II its α-enhanced counterpart (Pietrinferni et al. 2021), followed in Paper III by the extension of the library to the white dwarf regime (Salaris et al. 2022).[1]

In this paper (Paper IV of this series), we present a further extension of the new BaSTI library to cover chemical compositions with an α-depleted ([α/Fe] $= -0.20$) metal distribution. To the best of our knowledge, there are only two other stellar model and isochrone libraries for α-depleted chemical mixtures in the literature, published by Dotter et al. (2007) and VandenBerg et al. (2014).

The presence of α-depleted stars has been revealed by spectroscopic observations both in Local Group dwarf galaxies, as discussed in the classic review by Tolstoy, Hill & Tosi (2009) – see also the results by Vargas et al. (2013) for a sample of ultra-faint dwarfs, and Hill et al. (2019) for the Sculptor dwarf galaxy – and in the Milky Way (Nissen et al. 2020; Hayes et al. 2022; Wang et al. 2023). An accurate characterization of these populations of stars can indeed greatly benefit from stellar models and isochrones with the appropriate metal abundance distribution, given the sensitivity of the bolometric corrections (BCs) at optical and shorter wavelength to the specific metal abundance pattern (see Cassisi et al. 2004, and the next sections).

This paper is organized as follows. Section 2 summarizes the physics inputs and the heavy element distribution adopted in the calculations, followed by Section 3 that first presents the stellar

★ E-mail: adriano.pietrinferni@inaf.it , santi.cassisi@inaf.it
[1]All these libraries are publicly available at the new official BaSTI website: http://basti-iac.oa-abruzzo.inaf.it.

Table 1. The adopted α-depleted heavy element mixture.

Element	Mass fraction	Number fraction
C	0.238566	0.34146
N	0.063738	0.07823
O	0.364857	0.39204
Ne	0.093950	0.08004
Na	0.002955	0.00221
Mg	0.034963	0.02473
Al	0.005117	0.00326
Si	0.039486	0.02417
P	0.000559	0.00031
S	0.017940	0.00962
Cl	0.000412	0.00020
Ar	0.008319	0.00358
K	0.000318	0.00014
Ca	0.003404	0.00146
Ti	0.000167	0.00006
Cr	0.001543	0.00051
Mn	0.001118	0.00035
Fe	0.116168	0.03576
Ni	0.006419	0.00188

Table 2. Grid of initial chemical abundances.

[Fe/H]	[M/H]	Z	Y
0.45	0.33	0.03037	0.2867
0.30	0.18	0.02210	0.2759
0.15	0.03	0.01596	0.2679
0.06	−0.06	0.01309	0.2641
−0.08	−0.20	0.00959	0.2595
−0.20	−0.32	0.00733	0.2566
−0.30	−0.42	0.00585	0.2546
−0.40	−0.52	0.00466	0.2531
−0.60	−0.72	0.00296	0.2509
−0.70	−0.82	0.00235	0.2501
−0.90	−1.02	0.00149	0.2489
−1.05	−1.17	0.00106	0.2484
−1.20	−1.32	0.00075	0.2480
−1.30	−1.42	0.00059	0.2478
−1.40	−1.52	0.00047	0.2476
−1.55	−1.67	0.00033	0.2474
−1.70	−1.82	0.00024	0.2473
−1.90	−2.02	0.00015	0.2472
−2.20	−2.32	0.00007	0.2471
−2.50	−2.62	0.00004	0.2471
−3.20	−3.32	0.00001	0.2470

model grid and its mass, chemical composition, evolutionary phase coverage, and then shows comparisons with previous calculations available in the literature. Section 4 discusses the importance of using BCs calculated for the appropriate α-depleted metal mixture when comparing models and isochrones to data in colour–magnitude diagrams (CMDs), followed by a summary in Section 5.

2 METAL DISTRIBUTION AND PHYSICS INPUTS

For these calculations, we have employed the same stellar evolution code and physics inputs of Papers I and II. The adopted α-depleted metal distribution listed in Table 1 has been calculated with the α-elements O, Ne, Mg, Si, S, Ca, and Ti uniformly depleted with respect to Fe in comparison to the corresponding solar ratios (the reference solar-scaled metal distribution is from Caffau et al. 2011, as in Papers I and II) by 0.2 dex ($[\alpha/\mathrm{Fe}] = -0.2$).

This metal distribution has been employed consistently for the calculation of the nuclear energy generation, and radiative and electron conduction opacities, as well as in the equation of state (and BCs; see Section 4). The sources for all these physics inputs are given in Paper I, together with details about the treatment of the neutrino energy loss rates, superadiabatic convection (we employ a mixing length $\alpha_{\mathrm{ML}} = 2.006$ obtained from a solar model calibration), overshooting from the convective cores, and atomic diffusion (without radiative levitation). As for the outer boundary conditions, in the case of models with initial mass larger than about $0.5\,\mathrm{M}_{\odot}$ we used the integration of a $T(\tau)$ relation as in Papers I and II. At lower masses, i.e. in the range of very low mass stars, for both solar-scaled and α-enhanced models we used outer boundary conditions provided by model atmosphere computations (see Papers I and II for details). However, for our α-depleted calculations we have not been able to find publicly available outer boundary conditions from model atmospheres with the appropriate α-depleted metal mixture, consistent with those adopted for the other sets of models in the BaSTI-IAC library. We were therefore forced to use also for very low mass stars the integration of the same $T(\tau)$ relationship adopted for larger masses.

Mass-loss has been included by means of the Reimers (1975) formula, with the free parameter η set to 0.3 (see Papers I and II for details).

3 THE MODEL LIBRARY

To allow easy comparisons and interpolations with our solar-scaled and the α-enhanced libraries, the α-depleted models have been calculated for the same [Fe/H] values of the other two metal mixtures. For each assumed value of [Fe/H], we have derived the corresponding metallicity Z, and the associated He mass fraction (Y) adopting the helium-enrichment ratio ($\mathrm{d}Y/\mathrm{d}Z$) equal to 1.31 (see Paper I). Our model grid includes 21 metallicity values, listed in Table 2.

For each initial chemical composition, evolutionary sequences for 56 different values of the initial stellar mass have been computed: the minimum initial mass is $0.1\,\mathrm{M}_{\odot}$, while the maximum value is $15\,\mathrm{M}_{\odot}$. For initial masses below $0.2\,\mathrm{M}_{\odot}$, we computed evolutionary tracks for masses equal to 0.10, 0.12, 0.15, and $0.18\,\mathrm{M}_{\odot}$. In the range between 0.2 and $0.7\,\mathrm{M}_{\odot}$, a mass step equal to $0.05\,\mathrm{M}_{\odot}$ has been adopted. Mass steps equal to 0.1, 0.2, 0.5, and $1\,\mathrm{M}_{\odot}$ have been adopted for the mass ranges 0.7–2.6, 2.6–3, and 3–10 $\mathrm{M}_{\odot}$, and masses larger than $10\,\mathrm{M}_{\odot}$, respectively.

Models less massive than $4\,\mathrm{M}_{\odot}$ have been computed from the pre-main sequence (pre-MS), whereas more massive models have been computed starting from the zero-age MS configuration.

All stellar models – but those corresponding to very low mass stars whose core H-burning lifetime is much longer than the Hubble time – have been calculated until the start of the thermal pulses on the asymptotic giant branch, or C-ignition for the more massive ones. For the very low mass stars, the calculations have been stopped when the central H mass fraction is ≈0.3 (corresponding to ages already much older than the Hubble time). For each metallicity, an extended set of low-mass core He-burning models suitable for the study of the horizontal branch in old stellar populations has been also computed, as done in Papers I and II.

All the evolutionary sequences have been normalized, i.e. reduced to the same number of lines using the technique of ‘equivalent

Table 3. Available photometric systems. For each system, information about the source from the response curves and reference zero-points is provided.

Photometric system	Calibration	Passbands	Zero-points
2MASS	Vegamag	Cohen, Wheaton & Megeath (2003)	Cohen, Wheaton & Megeath (2003)
CFHT (MegaCam)	ABmag	CFHT Documentation[a]	0
Euclid (VIS + NISP)	ABmag	Euclid mission data base[b]	0
Gaia DR1	Vegamag	Jordi et al. (2010)[c]	Jordi et al. (2010)
Gaia DR2	Vegamag	Maíz Apellániz & Weiler (2018)[d]	Maíz Apellániz & Weiler (2018)
Gaia DR3	Vegamag	Riello et al. (2021)	Riello et al. (2021)
GALEX	ABmag	NASA[e]	0
Hipparcos + Thyco	ABmag	Bessell & Murphy (2012)	Bessell & Murphy (2012)
HST (WFPC2)	Vegamag	SYNPHOT	SYNPHOT
HST (WFC3)	Vegamag	SYNPHOT	SYNPHOT
HST (ACS)	Vegamag	SYNPHOT	SYNPHOT
Johnson, Bessel & Brett	Vegamag	Bessell & Brett (1988), Bessell (1990)	Bessell, Castelli & Plez (1998)
J-PLUS	ABmag	J-PLUS Collaboration[f]	0
JWST (NIRCam – post launch)	Vegamag	JWST User Documentation[g]	SYNPHOT
JWST (NIRCam – Sirius)[h]	Vegamag	JWST User Documentation[g]	SYNPHOT
JWST (NIRISS – post launch)	Vegamag	JWST User Documentation[g]	SYNPHOT
Kepler	ABmag	Kepler Collaboration[i]	0
Nancy Grace Roman Telescope (WFI)	Vegamag	Roman Documentation[j]	SYNPHOT
PanSTARSS1	ABmag	Tonry et al. (2012)	0
SAGE	ABmag	SAGE Collaboration	0
SDSS	ABmag	Doi et al. (2010)	Dotter et al. (2008)
Skymapper	ABmag	Bessell (2011)	0
Spitzer (IRAC)	Vegamag	NASA[k]	Groenewegen (2006)
Strömgren	Vegamag	Maíz Apellániz (2006)	Maíz Apellániz (2006)
Subaru (HSC)	ABmag	HSC Collaboration[l]	0
SWIFT (UVOT)	Vegamag	HEASARC[m]	Poole et al. (2008)
TESS	ABmag	TESS Collaboration[n]	0
UVIT (FUV + NUV + VIS)	ABmag	UVIT Collaboration[o]	Tandon et al. (2017)
Vera C. Rubin Observatory	ABmag	LSST Collaboration[p]	0
Victor M. Blanco Telescope (DECam)	ABmag	CTIO[q]	0
VISTA (VIRCAM)	Vegamag	ESO[r]	Rubele et al. (2012)
WISE	Vegamag	WISE Collaboration[s]	Wright et al. (2010)

[a] https://www.cfht.hawaii.edu/Instruments/Filters/megaprimenew.html
[b] http://euclid.esac.esa.int/epdb/db/SPV02/SPV02/EUC_MDB_MISSIONCONFIGURATION-SPV02_2018-06-16T140000.00Z_01.01.xml.html
[c] The nominal G passband curve has been corrected following the post-DR1 correction provided by Maíz Apellániz (2017).
[d] Two different G_{BP} passbands are provided for sources brighter and fainter than $G = 10.87$, respectively.
[e] https://asd.gsfc.nasa.gov/archive/galex/Documents/PostLaunchResponseCurveData.html
[f] http://www.j-plus.es/survey/instrumentation
[g] https://jwst-docs.stsci.edu/
[h] This photometric system adopts the 'post launch passbands but Vega zero-points obtained by using Sirius as the colour reference (see JWST User Documentation for more details).
[i] https://nexsci.caltech.edu/workshop/2012/keplergo/CalibrationResponse.shtml
[j] https://roman.gsfc.nasa.gov/science/WFI_technical.html
[k] https://irsa.ipac.caltech.edu/data/SPITZER/docs/irac/calibrationfiles/spectralresponse/
[l] https://hsc-release.mtk.nao.ac.jp/doc/index.php/survey/
[m] https://heasarc.gsfc.nasa.gov/docs/heasarc/caldb/data/swift/uvota/index.html
[n] https://heasarc.gsfc.nasa.gov/docs/tess/data/tess-response-function-v1.0.csv
[o] https://uvit.iiap.res.in/Instrument/Filters
[p] https://github.com/lsst/throughputs/tree/master/baseline
[q] http://www.ctio.noirlab.edu/noao/content/decam-filter-information
[r] http://www.eso.org/sci/facilities/paranal/instruments/vircam/inst/
[s] https://wise2.ipac.caltech.edu/docs/release/prelim/expsup/sec4_3g.html#WISEZMA

points' as described in Papers I and II.[2] For consistency, the same criterion has been applied to the solar-scaled and α-enhanced models in the library and used for computing isochrones in a wide age range.

Having evolutionary tracks and isochrones computed this way, with the same number of points together with the homogeneous [Fe/H] grid for solar-scaled, α-enhanced, and α-depleted calculations, makes it easy to calculate evolutionary tracks and/or isochrones at fixed [Fe/H] for any arbitrary value of [α/Fe] between -0.2 and $+0.4$ dex. One could use, for example, a parabola to

[2] Although the normalization procedure is exactly the same as that adopted in Hidalgo et al. (2018), we have slightly modified the definition of one of the selected key points to better account for the extremely long evolutionary time-scales of very low mass stars. More in detail, the fourth key point for these models now corresponds to the evolutionary stage when H burning has decreased the central hydrogen mass fraction by 0.01 with respect to the initial value.

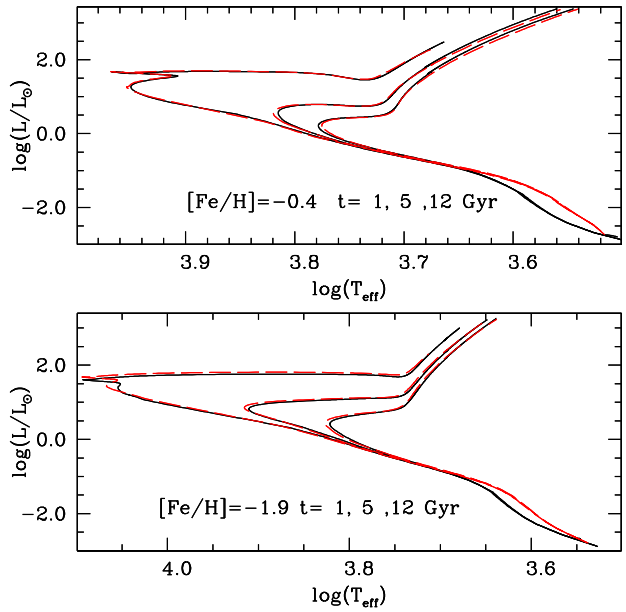

Figure 1. Comparison between Dotter et al. (2007) and our [α/Fe] = −0.2 isochrones from the MS to the tip of the RGB (red dashed and black solid lines, respectively) with the labelled [Fe/H] and ages.

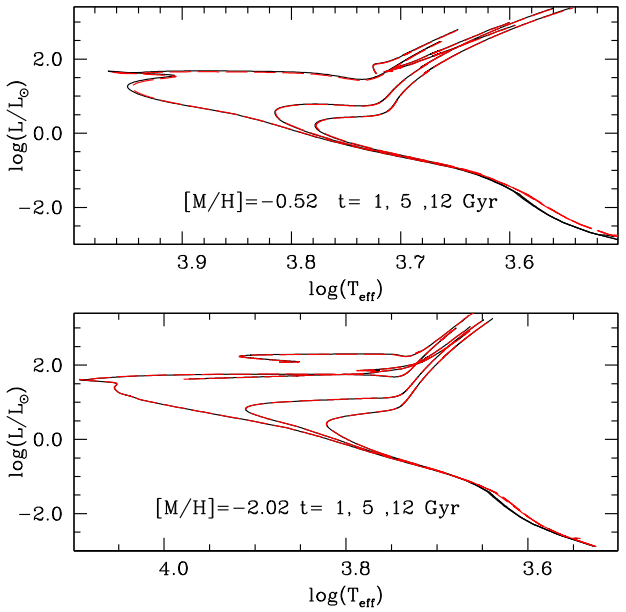

Figure 2. Comparison in the HRD between our α-depleted (black solid lines) and solar-scaled (Hidalgo et al. 2018) isochrones (red dashed lines) with the labelled total metallicities [M/H] and ages.

interpolate in [α/Fe] point by point along the tracks and isochrones. The same is true also for interpolations in [Fe/H] at a given [α/Fe].

Both evolutionary tracks and isochrones are provided in the theoretical Hertzsprung–Russell diagram (HRD) and in various photometric systems as described in Papers I and II, by applying BCs obtained from theoretical spectra (consistent with those employed in Papers I and II) calculated with the appropriate α-depleted metal distribution. However, due to the lack of suitable α-depleted synthetic spectra for VLM stars, in this mass regime we have been forced to adopt a different approach. For each value of [Fe/H], we have employed the solar-scaled BCs of Paper I after applying – for each photometric filter – a shift in order to match the corresponding BC at $T_{\rm eff} \approx 5000$ K and $\log g = 4.5$ provided by the α-depleted synthetic spectra obtained with the ATLAS9 code (see the discussion in Paper I).

Several photometric systems have been added (or updated) since the publication of Paper I, and Table 3 shows an updated list of the systems available in our model library for α-enhanced, solar-scaled, and α-depleted calculations.

Fig. 1 shows the HRD of our 1, 5 and 12 Gyr isochrones for two values of [Fe/H], compared to the corresponding Dotter et al. (2007) α-depleted isochrones [we could not compare with the calculations by VandenBerg et al. (2014), because they are for a 0.4 dex α depletion], from the MS to the tip of the red giant branch (RGB)[3] Dotter et al. (2007) calculations employ a metal distribution with [α/Fe] = −0.20 as in our models, although the reference solar mixture [the Grevesse & Sauval (1998), solar metal composition is used by these authors] is not the same, and there are differences also in some physics inputs (see Dotter et al. 2007, for details).

Apart from the lower MS, the two sets of isochrones are in close agreement. Differences in $T_{\rm eff}$ at fixed luminosity are at most by a few tens of K, and the Turn Off (TO) luminosities are always practically the same, apart from the 1 and 5 Gyr, [Fe/H] = −1.9 cases, with the Dotter et al. (2007) isochrones showing a slightly brighter TO than our calculations, corresponding to an age difference by about 100 Myr.

The disagreement between the two sets of models along the fainter portion of the MS is due to the use of different approaches for the outer boundary conditions, an input that significantly affects the $T_{\rm eff}$ scale of very low mass stars, as well as to differences in the adopted chemical mixtures (see below for more details).

4 THE ROLE OF THE BOLOMETRIC CORRECTIONS

As shown by Cassisi et al. (2004) and confirmed by our more recent calculations (Pietrinferni et al. 2021), α-enhanced isochrones with ages above ∼1 Gyr can be well mimicked by solar-scaled ones with the same total metallicity [M/H] not only in the HRD, but also in *VI* and infrared CMDs, while the agreement is less satisfactory in optical CMDs and worsens at shorter wavelengths. The good match in the HRD confirms the results of the pioneering study by Salaris, Chieffi & Straniero (1993), who at the time did not have available BCs calculated with a consistent α-enhanced metal distribution. Indeed, the poorer agreement in CMDs at optical and shorter wavelengths is due to differences in the BCs induced by the effect of the change in the metal abundance distribution on the stellar spectra.

We expect that similar results should hold also when comparing α-depleted with solar-scaled isochrones at the same [M/H], and indeed this is the case, as shown in Fig. 2.

Here, we compare our α-depleted 1, 5, and 12 Gyr isochrones with the solar-scaled ones from Hidalgo et al. (2018) at two different common values of [M/H]. There is a perfect match between the two pairs of isochrones along MS, TO, and the core He-burning phase after the He flash at the tip of the RGB. Differences appear only on the lower MS for $\log(L/L_\odot)$ below ∼−1.0 corresponding to masses below ∼0.5 $M_\odot$. Similar differences for the very low mass

[3]These isochrones have been computed using the online interpolation tool at http://stellar.dartmouth.edu/models/isolf_new.html.

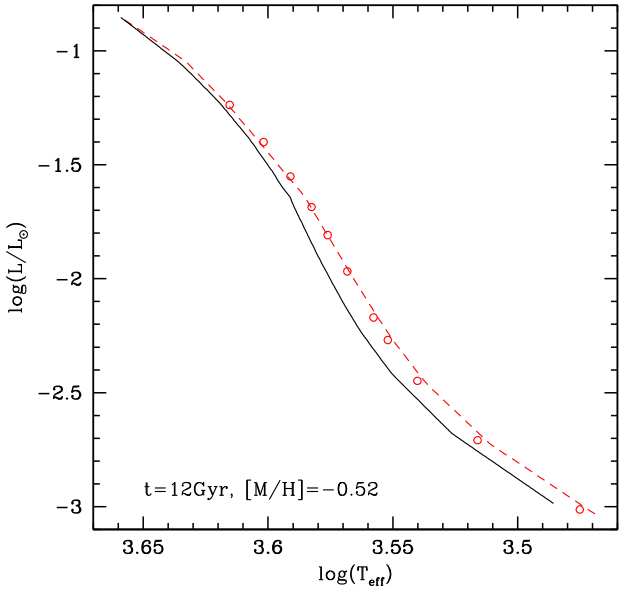

Figure 3. Comparison in the HRD between α-depleted (black solid lines) and solar-scaled (Hidalgo et al. 2018) isochrones (red dashed lines) for the labelled values of the total metallicity and age. The open dots denote solar-scaled models with mass between 0.1 and 0.5 $M_\odot$ for the same values of [M/H] and age, but computed employing for the outer boundary conditions the same $T(\tau)$ relationship adopted for the α-depleted calculations.

regime were found in Paper II when comparing solar-scaled (from Paper I) with α-enhanced models. To verify the role played by the outer boundary conditions in causing these differences, we computed solar-scaled stellar models in this mass regime for [M/H] $= -0.52$, by adopting the same $T(\tau)$ relationship used for our α-depleted computations. Fig. 3 shows the resulting 12 Gyr isochrone compared to our new α-depleted calculations, and a solar-scaled one from Paper I models. When comparing the two solar-scaled isochrones, it is easy to notice that the use of a $T(\tau)$ relationship instead of the more appropriate boundary conditions provided by model atmospheres employed in Paper I calculations, makes the very low mass models hotter (see also Baraffe et al. 1997; Cassisi et al. 2000, and references therein). However, the impact is not able to explain the full difference between our solar-scaled calculations and the α-depleted ones at the same [M/H] (the same is true for the differences with the α-enhanced models shown in Paper II). Indeed, the main source of these $T_{\rm eff}$ differences is not so much the way the boundary conditions are computed, rather the metal mixture used in their calculations. As already discussed by VandenBerg et al. (2022) and VandenBerg (2023), the boundary conditions are much more sensitive to the adopted specific metal abundance distribution than for more massive models. In particular, VandenBerg (2023) has demonstrated the crucial role played by oxygen – whose abundance changes substantially when moving from the solar-scaled mixture to the α-depleted/enhanced ones – in determining the atmospheric thermal stratification of very low mass stars. The differences in the boundary conditions for very low mass models at a given total metallicity are the primary reason for the $T_{\rm eff}$ differences between solar-scaled and α-depleted isochrones shown in Fig. 3.

Fig. 4 highlights the effect of the α-depleted heavy element distribution of the model BCs, the same way it was shown by Cassisi et al. (2004) for the α-enhanced case. We display here 12 Gyr, [Fe/H] $= -0.7$ α-depleted isochrones in different CMDs, calculated using the appropriate BCs for a consistent α-depleted metal mixture (we denote them as self-consistent isochrones), BCs calculated for a solar-scaled metal mixture and the same [Fe/H] of the isochrone (denoted as [Fe/H] isochrones), and BCs computed for a solar-scaled metal mixture and the same [M/H] of the isochrone (denoted as [M/H] isochrones). We do not show the lower MS, for which we do not have models computed using boundary conditions from α-depleted model atmospheres.

As in Cassisi et al. (2004), we find that the perfect agreement between the three isochrones in the infrared CMD progressively worsens, especially at low $T_{\rm eff}$, when moving to CMDs at increasingly shorter wavelengths. Moreover, these differences quantitatively decrease with decreasing [Fe/H] of the self-consistent α-depleted isochrone.

Just for reference, in the *UB* CMD the RGB at $M_U = 3$ for the [M/H] isochrone is 0.08 mag bluer than the self-consistent one, while the [Fe/H] solar-scaled isochrone is 0.03 mag bluer. The absolute U magnitude and $(U - B)$ colour of the TO are the same for the self-consistent and the [Fe/H] isochrone, while M_U is ∼0.03 mag fainter and $(U - B)$ is 0.02 mag bluer for the [M/H] isochrone. On the MS at $M_U = 9$, the [M/H] isochrone is 0.07 mag bluer than the self-consistent one, while the [Fe/H] solar-scaled isochrone is 0.04 mag bluer. These differences are substantially larger when considering magnitudes and colours in the UV wavelength range.

Moving to the *BV* CMD, the differences decrease. On the RGB at $M_V = 1$, the [M/H] isochrone is now 0.04 mag bluer than the self-consistent one, while the [Fe/H] isochrone is 0.02 mag bluer. The TO colours and magnitudes are basically identical among the three isochrones, while on the MS at $M_V = 7.5$ the [M/H] isochrone is 0.06 mag bluer than the self-consistent one and the [Fe/H] solar-scaled isochrone is 0.05 mag bluer. In the *VI* CMD, differences appear only when approaching the tip of the RGB, which is redder in both [Fe/H] and [M/H] isochrones by about 0.12 mag.

On average, the [Fe/H] isochrone is a better approximation of the self-consistent one, in agreement with the results by Cassisi et al. (2004) for the α-enhanced regime. Not surprisingly, the sign of the colour differences is the opposite of the α-enhanced comparison, whereby the [Fe/H] and [M/H] isochrones are redder along the RGB and the MS. As discussed briefly in Cassisi et al. (2004), the different abundances of mainly O, Si, Mg, and Ca between α-depleted and solar-scaled compositions affect both the line opacity and the continuum opacity in the atmospheres, causing a redistribution of the flux among the various wavelengths, and a change of the values of the BCs at fixed $T_{\rm eff}$ and gravity.

5 SUMMARY

We have presented our new BaSTI α-depleted ([α/Fe] $= -0.20$) stellar models and isochrones, suitable to investigate the evolutionary properties of the α-depleted populations discovered in the Milky Way and Local Group dwarfs. The models have been calculated with the same physics inputs and reference solar metal mixture employed for our updated solar-scaled and α-enhanced ([α/Fe] $= 0.4$) calculations published in Papers I and II, and cover the same mass and [Fe/H] ranges.

We have compared the HRDs of selected α-depleted isochrones with the Dotter et al. (2007) [α/Fe] $= -0.20$ counterparts, from the MS to the tip of the RGB, finding an overall good agreement despite differences in the reference solar mixture and some physics inputs. We have also discussed the importance of employing BCs calculated for the appropriate α-depleted heavy element mixture

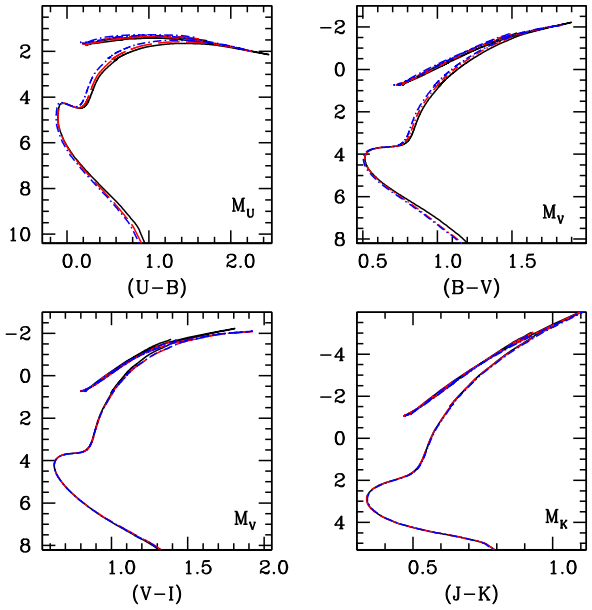

Figure 4. Comparison in various CMDs of a self-consistent 12 Gyr, [Fe/H] = −0.7 α-depleted isochrone (black solid lines), with isochrones for the same age and chemical composition but calculated using solar-scaled BCs with either the same [Fe/H] (red dashed lines) or the same [M/H] (blue dash–dotted lines) of the self-consistent isochrone, respectively. We did not display the portion of the isochrones populated by masses below $\sim$0.5 $M_\odot$ (see the text for details).

when comparing isochrones (and evolutionary tracks) to data in optical CMDs and at shorter wavelengths.

Like for the solar-scaled and α-enhanced libraries, these new α-depleted evolutionary tracks and isochrones are available in several photometric systems at http://basti-iac.oa-abruzzo.inaf.it. In the near future, we will make available on the BaSTI website an online tool to interpolate among our sets of calculations, to obtain tracks and isochrones in all available photometric filters for any value of [α/Fe] between −0.2 and +0.4.

ACKNOWLEDGEMENTS

We warmly thank our anonymous referee for pointing out the origin of the differences between our sets of very low mass models computed with different heavy element mixtures. SC and AP acknowledge support from PRIN-MIUR2022 (PI: S. Cassisi), INAF Theory grant 'Lasting' (PI: S. Cassisi), INFN (Iniziativa specifica TAsP), and PLATO ASI-INAF agreement no. 2015-019-R.1-2018. MS acknowledges support from STFC Consolidated Grant ST/V00087X/1.

DATA AVAILABILITY

The α-depleted evolutionary tracks and isochrones in several photometric systems are publicly available at the new official BaSTI website: http://basti-iac.oa-abruzzo.inaf.it.

REFERENCES

Baraffe I., Chabrier G., Allard F., Hauschildt P. H., 1997, A&A, 327, 1054
Bessell M. S., 1990, PASP, 102, 1181
Bessell M. S., 2011, in Qain S., Leung K., Zhu L., Kwok S., eds, ASP Conf. Ser. Vol. 451, Science with the Skymapper Telescope. Astron. Soc. Pac., San Francisco, p. 323
Bessell M. S., Brett J. M., 1988, PASP, 100, 1134
Bessell M., Murphy S., 2012, PASP, 124, 140
Bessell M. S., Castelli F., Plez B., 1998, A&A, 333, 231
Caffau E., Ludwig H. G., Steffen M., Freytag B., Bonifacio P., 2011, Sol. Phys., 268, 255
Cassisi S., Castellani V., Ciarcelluti P., Piotto G., Zoccali M., 2000, MNRAS, 315, 679
Cassisi S., Salaris M., Castelli F., Pietrinferni A., 2004, ApJ, 616, 498
Cohen M., Wheaton W. A., Megeath S. T., 2003, AJ, 126, 1090
Doi M. et al., 2010, AJ, 139, 1628
Dotter A., Chaboyer B., Jevremović D., Baron E., Ferguson J. W., Sarajedini A., Anderson J., 2007, AJ, 134, 376
Dotter A., Chaboyer B., Jevremović D., Kostov V., Baron E., Ferguson J. W., 2008, ApJS, 178, 89
Grevesse N., Sauval A. J., 1998, Space Sci. Rev., 85, 161
Groenewegen M. A. T., 2006, A&A, 448, 181
Hayes C. R. et al., 2022, ApJS, 262, 34
Hidalgo S. L. et al., 2018, ApJ, 856, 125
Hill V. et al., 2019, A&A, 626, A15
Jordi C. et al., 2010, A&A, 523, A48
Maíz Apellániz J., 2006, AJ, 131, 1184
Maíz Apellániz J., 2017, A&A, 608, L8
Maíz Apellániz J., Weiler M., 2018, A&A, 619, A180
Nissen P. E., Christensen-Dalsgaard J., Mosumgaard J. R., Silva Aguirre V., Spitoni E., Verma K., 2020, A&A, 640, A81
Pietrinferni A. et al., 2021, ApJ, 908, 102
Poole T. S. et al., 2008, MNRAS, 383, 627
Reimers D., 1975, Mem. Soc. R. Sci. Liege, 8, 369
Riello M.,Angeli De, W. Evans D., et al., 2021, A&A,649, A3
Rubele S. et al., 2012, A&A, 537, A106
Salaris M., Chieffi A., Straniero O., 1993, ApJ, 414, 580
Salaris M., Cassisi S., Pietrinferni A., Hidalgo S., 2022, MNRAS, 509, 5197
Tandon S. N. et al., 2017, J. Astrophys. Astron., 38, 28
Tolstoy E., Hill V., Tosi M., 2009, ARA&A, 47, 371
Tonry J. L. et al., 2012, ApJ, 750, 99
VandenBerg D. A., 2023, MNRAS, 518, 4517
VandenBerg D. A., Bergbusch P. A., Ferguson J. W., Edvardsson B., 2014, ApJ, 794, 72
VandenBerg D. A., Edvardsson B., Casagrande L., Ferguson J. W., 2022, MNRAS, 509, 4189
Vargas L. C., Geha M., Kirby E. N., Simon J. D., 2013, ApJ, 767, 134
Wang R., Luo A.-L., Zhang S., Ting Y.-S., O'Briain T., LAMOST MRS Collaboration, 2023, ApJS, 266, 40
Wright E. L. et al., 2010, AJ, 140, 1868

This paper has been typeset from a TEX/LATEX file prepared by the author.